Impact of Ion Binding on Poly-L-Lysine (Un)folding Energy Landscape and Kinetics
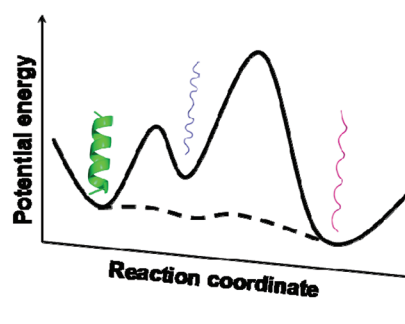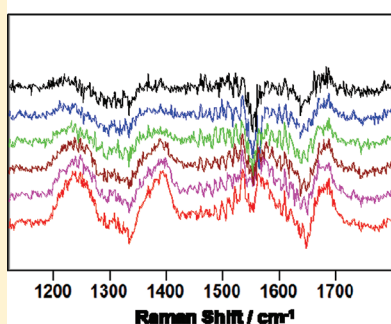
Kan Xiong[†,‡] and Sanford A. Asher*[,†]

[†]Department of Chemistry, University of Pittsburgh, Pittsburgh, Pennsylvania 15260, United States

S *Supporting Information*

ABSTRACT: We utilize T-jump UV resonance Raman spectroscopy (UVRR) to study the impact of ion binding on the equilibrium energy landscape and on (un)folding kinetics of poly-L-lysine (PLL). We observe that the relaxation rates of the folded conformations (including π-helix (bulge), pure α-helix, and turns) of PLL are slower than those of short alanine-based peptides. The PLL pure α-helix folding time is similar to that of short alanine-based peptides. We for the first time have directly observed that turn conformations are α-helix and π-helix (bulge) unfolding intermediates. ClO_4^- binding to the Lys side chain $-NH_3^+$ groups and the peptide backbone slows the α-helix unfolding rate compared to that in pure water, but little impacts the folding rate, resulting in an increased α-helix stability. ClO_4^- binding significantly increases the PLL unfolding activation barrier but little impacts the folding barrier. Thus, the PLL folding coordinate(s) differs from the unfolding coordinate(s). The π helix (bulge) unfolding and folding coordinates do not directly go through the α-helix energy well. Our results clearly demonstrate that PLL (un)folding is not a two-state process.

■ INTRODUCTION

The α-helix is the most common secondary structural element of proteins. Elucidating the mechanism(s) of α-helix melting and refolding is essential for understanding protein folding. Despite extensive studies over the past 50 years, the mechanism(s) by which α-helices melt and refold is still poorly understood.[1−7]

The current understanding of α-helix (un)folding kinetics mainly derives from extensive studies of alanine-based peptides.[8−20] These studies show relaxation rates in the 100−400 ns range depending on the peptide length,[21] the temperature,[10,15−18] the terminal capping species,[21] the location on the α-helix peptide,[10,18] and the solution environment (such as pH and ionic strength[22,23]).

In this work, we utilize T-jump UVRR to study the impact of $NaClO_4$ on the Gibbs free energy landscape and on the (un)folding kinetics of PLL. The equilibrium conformational transitions of PLL have been characterized by numerous techniques.[24−28] However, little is known about the accompanying conformational dynamics.

We utilize T-jump UVRR to monitor the PLL secondary structure evolution during unfolding. We for the first time have experimentally observed that turn conformations are α-helix

and π-helix (bulge) unfolding intermediates. In 0.5 M $NaClO_4$ at 40 °C (pH 10.66), the π-helix (bulge) melts faster than the pure α-helix. ClO_4^- binding to Lys side chain $-NH_3^+$ groups and the peptide bond slows α-helix unfolding but little impacts folding, resulting in an increased α-helix stability. It appears that ClO_4^- increases the PLL unfolding activation barrier but little impacts the folding barrier. This may indicate that ClO_4^- preferentially binds to PLL folded conformations, decreasing the energies of the folded conformations (the α-helix-like conformations) relative to the energies of the unfolded PPII and 2.5_1-helix conformations.

■ EXPERIMENTAL DETAILS

Materials. Poly-L-lysine HCl (M_{vis} = 20 900, DP_{vis} = 127, M_{MALLS} = 11400, DP_{MALLS} = 69; DP_{vis} and DP_{MALLS} refer to the degree of polymerization measured by viscosity and multiangle laser light scattering, respectively) was purchased from Sigma and used without further purification. $NaClO_4$ was purchased from Sigma.

T-jump UV Raman Measurements. The UVRR spectrometer was described in detail by Bykov et al.[29] Briefly, 204 nm UV light (3 ns pulse width, ~1 mW average power, ~200 μm spot size) was obtained by generating the fifth anti-Stokes Raman harmonic of the third harmonic of a Nd:YAG laser (Coherent, Infinity). The peptide solution was circulated in a free surface, temperature-controlled stream. A 165° sampling backscattering geometry was used. The collected light was dispersed by a double monochromator onto a back thinned CCD camera with a Lumogen E coating (Princeton Instruments-Spec 10 System). We averaged three 10-min accumulations.

To selectively heat the water solvent, we Raman-shifted the 1064 nm Nd:YAG fundamental to 1.9 μm by using a 1 m Raman shifter (Light Age Inc.; 600 psi H_2) to obtain ~1.5 mJ pulse energies at a 90 Hz repetition rate. This 1.9 μm excitation is absorbed by a water combination band, and the energy is thermalized within picoseconds by vibrational relaxation.[30]

We performed T-jump measurements from 10 to ~40 °C and from 20 to ~50 °C. The magnitudes of the T-jumps were determined by measuring the temperature sensitive water stretching bands (see Figures S1−4 in the Supporting Information for details). These T-jumps were obtained by focusing the 1.9 μm laser pulses to a ~300 μm diameter spot in the flowing sample stream. To ensure that the Raman signal was obtained from the sample volume maximally heated by the IR pulses, we adjusted the sample absorbance at 204 nm to ~40 cm^{-1} by using a 15 mg/mL peptide concentration in T-jump studies of PLL in pure water. In T-jump studies of PLL in 0.5 M NaClO$_4$, we decreased the peptide concentration to 5 mg/mL to minimize aggregation. To achieve the same 204 nm sample absorption as that of the 15 mg/mL PLL sample, we included 0.015 M NaBr that has a molar absorptivity of 5700 M^{-1} cm^{-1} at 204 nm, which is six times that of the peptide bond[17] (see Figure S5 in the Supporting Information).

■ RESULTS

Static UVRR. Figure 1a shows the temperature dependence of the 204 nm excited UVRR spectra of PLL in 0.5 M NaClO$_4$ at pH 10.65. The 10 °C spectrum shows an AmI band at 1650 cm^{-1} (mainly CO stretching[31]), an AmII band at 1555 cm^{-1} (mainly out of phase combination of CN stretching and NH bending[31]), and (C)C$_\alpha$−H bending bands at 1392 cm^{-1}. The AmIII$_3$ bands (mainly in phase combination of CN stretching and NH bending[31]) occur between ~1200 and ~1280 cm^{-1}.

As the temperature increases, the AmI band frequency upshifts, indicating decreased hydrogen bonding of the carbonyls at higher temperatures.[32] The C$_\alpha$−H band intensity significantly increases with increasing temperature, indicating α-helix melting.[33] The AmIII$_3$ band frequency downshifts, and its intensity significantly increases, which also indicate α-helix melting.[34] UVRR spectra of PLL in pure water at pH 10.65 also indicate α-helix melting as the temperature increases (see Figure S6 in the Supporting Information).

We calculated the fractions of α-helix-like conformations of PLL at different temperatures by using the methodology of Ma et al.[24] The melting curve for PLL at pH 10.65 in pure water (Figure 1b) shows a melting temperature, T_m, of ~15 °C. Upon addition of 0.5 M NaClO$_4$, the α-helical fractions significantly increase, and T_m increases to >50 °C.

Kinetic UVRR of PLL in NaClO$_4$. Figure 2 shows T-jump difference UVRR spectra of PLL in 0.5 M NaClO$_4$ (pH 10.66) at different delay times between the pump and probe laser
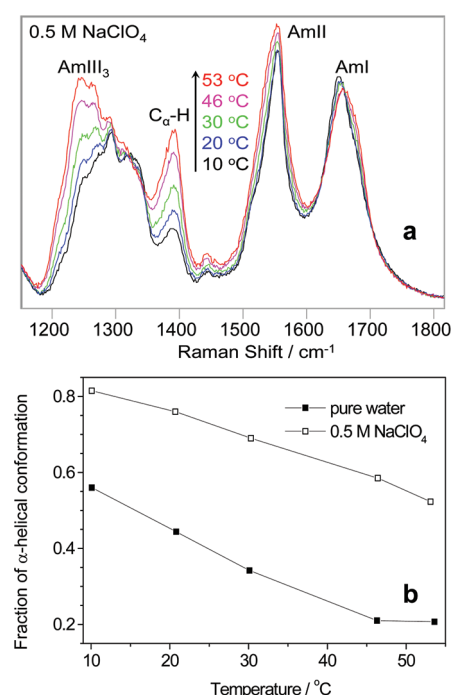

Figure 1. (a) Temperature dependence of the 204 nm excited UVRR spectra of 1 mg/mL PLL in 0.5 M NaClO$_4$ at pH 10.65. All spectra were normalized to the 932 cm^{-1} ClO$_4^-$ peak height. (b) Calculated fractions of α-helix-like conformations of PLL in 0.5 M NaClO$_4$ and in pure water at pH 10.65.
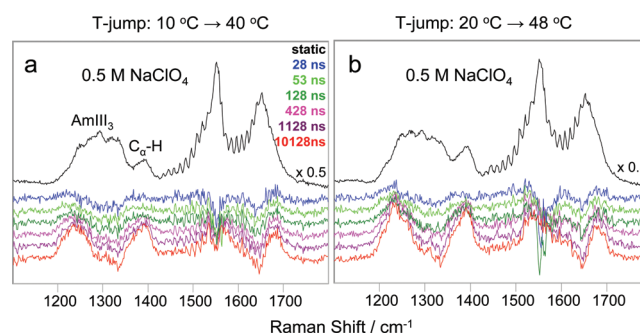

Figure 2. T-jump difference UVRR spectra of PLL in 0.5 M NaClO$_4$ (pH 10.66) at different delay times between the pump and probe laser pulses. These difference spectra were obtained by subtracting the static initial temperature spectrum from each of the longer delay time spectra. (a) Difference spectra for a 10 to 40 °C T-jump. (b) Difference spectra for a 20 to 48 °C T-jump. All spectra were normalized to the 932 cm^{-1} ClO$_4^-$ peak height before spectral subtraction. The oscillations centered at ~1550 cm^{-1} result from the rotational bands of oxygen[35,36] and occur due to the fact that UV light is focused near the surface of the flow stream where the oxygen concentration is high.

pulses. The 28 ns difference spectra show small positive features in the AmIII$_3$ and C$_\alpha$−H regions, indicating slight α-helix melting.[24] These features increase as the delay time increases.

Transient Ψ Distributions. We calculated the delay time dependent Ramachandran Ψ probability distributions for PLL by using the methodology of Ma et al.[24] Figure 3 shows Ramachandran Ψ probability distributions for PLL at 10 and 20 °C in 0.5 M NaClO$_4$ (pH 10.66). The static 10 °C Ψ distribution shows dominant contributions of the π-helix
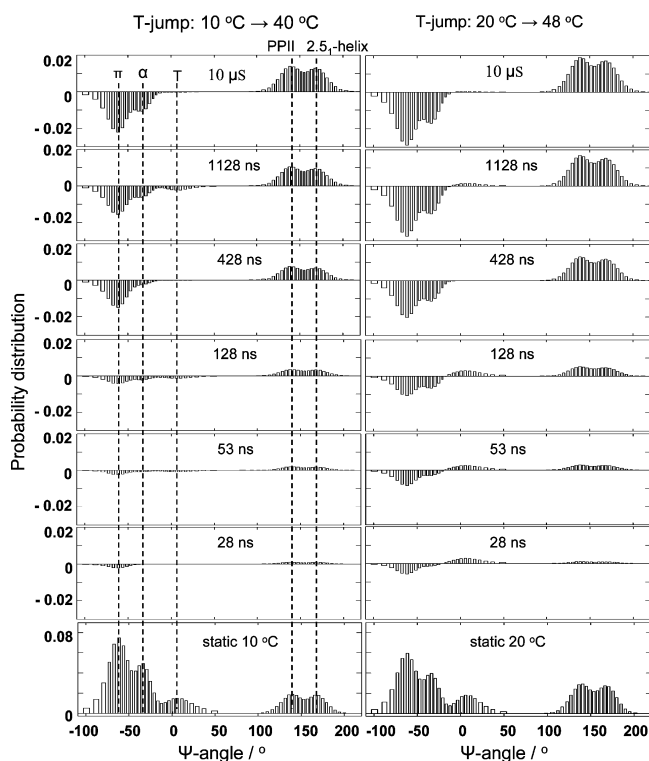
Figure 3. Ramachandran Ψ probability distributions for PLL at 10 and 20 °C in 0.5 M NaClO$_4$ (pH 10.66). Delay time dependent difference Ramachandran Ψ probability distributions for PLL in 0.5 M NaClO$_4$ (pH 10.66). These difference Ψ distributions were obtained by subtracting the static initial temperature Ψ distribution from each of the longer delay time Ψ distributions. π: π-helix (bulge). α: pure α-helix. T: turns.

(bulge) (Ψ ∼ −70 °), the pure α-helix (Ψ ∼ −40 °), and type I/I′ or type II/II′ β turns (Ψ ∼ 5 °). It also contains contributions of the polyproline II (PPII)-like (Ψ ∼ 140 °) and 2.5$_1$-helix (Ψ ∼ 170 °) conformations.

For the 10 to 40 °C T-jump, the difference distributions show that the π-helix (bulge) concentration slightly decreases at 28 ns and further decreases at longer delay times. The pure α-helix concentration does not decrease until 53 ns. The turn concentration starts decreasing at 128 ns, then increases at 428 ns, and decreases again at 1128 ns (Figure 4). The PPII and 2.5$_1$-helix concentrations monotonically increase as the delay time increases.
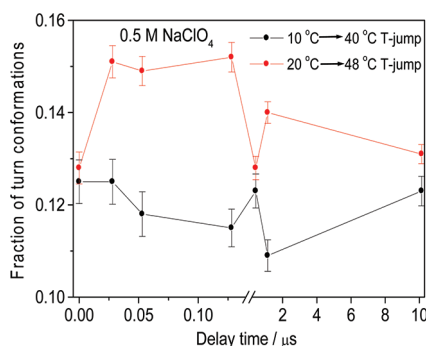

Figure 4. Delay time dependent fractions of turn conformations of PLL in 0.5 M NaClO$_4$ at pH 10.66.

The static 20 °C Ψ distribution shows decreased α-helix-like concentrations and increased PPII and 2.5$_1$-helix concentrations, compared to that at 10 °C (Figure 3). For the 20 to 48 °C T-jump, the π-helix (bulge) and pure α-helix concentrations decrease at 28 ns and further decrease at longer delay times. The turn concentration starts increasing at 28 ns, then decreases at 428 ns, and increases again at 1128 ns (Figure 4). The PPII and 2.5$_1$-helix concentrations monotonically increase as the delay time increases.

Relaxation Rates. Figure 5 shows monoexponential fits, $\Delta f = 1 - \exp(-t/\tau)$ (where Δf is the relative change at the different delay time) to the 0.5 M NaClO$_4$ (pH 10.66) relaxation of the integrated C$_\alpha$–H band intensities (that result from the extended PPII and 2.5$_1$-helix conformations of PLL[24]) (Figure 5a), the α-helix-like (π + α + T) concentrations (Figure 5b), the pure α-helix concentrations (Figure 5c), and the π-helix (bulge) concentrations (Figure 5d) of PLL.

The C$_\alpha$–H band intensities were determined by integrating the UVRR spectral intensities from 1370 to 1410 cm^{-1} at the different delay time. The α-helix-like, the pure α-helix, and the π-helix (bulge) concentrations were determined by integrating the Figure 3 Ψ probabilities between Ψ = 50° and −100°, between Ψ = −15° and −48°, and between Ψ = −48° and −100° at the different delay time, respectively.

We find a C$_\alpha$–H relaxation time for the 10 to 40 °C T-jump of 660 ± 70 ns, whereas for the 20 to 48 °C T-jump the relaxation time is 430 ± 40 ns. We also find an α-helix-like relaxation time for the 10 to 40 °C T-jump of 620 ± 70 ns, whereas for the 20 to 48 °C T-jump, the relaxation time is 390 ± 20 ns. The pure α-helix relaxation time for the 10 to 40 °C T-jump is 1360 ± 170 ns, whereas for the 20 to 48 °C T-jump, the relaxation time is 350 ± 40 ns. The π-helix (bulge) relaxation time for the 10 to 40 °C T-jump is 530 ± 100 ns, whereas for the 20 to 48 °C T-jump, the relaxation time is 280 ± 40 ns.

Kinetic Parameters. We calculated the kinetic parameters based on a two-state model for the α-helix-like conformations, the pure α-helix, and the π-helix (bulge) (un)folding. Table 1 shows that the reciprocals of the 0.5 M NaClO$_4$ (pH 10.66) PLL pure α-helix unfolding rate constants are 2020 ± 250 ns (at 40 °C) and 420 ± 50 ns (at 48 °C), while the reciprocals of the folding rate constants are 4100 ± 510 ns (at 40 °C) and 2090 ± 230 ns (at 48 °C).

We calculated the pure α-helix (un)folding activation energies by using the Arrhenius equation:

$$\ln\left(\frac{k(T_1)}{k(T_2)}\right) = -\frac{G^{\ddagger}}{R}\left(\frac{1}{T_1} - \frac{1}{T_2}\right) \tag{1}$$

where k is the rate constant and $G^{\ddagger}$ is the activation energy. The calculated pure α-helix unfolding activation energy is 17.2 ± 4.2 kcal/mol, while the folding activation energy is 40.4 ± 4.2 kcal/mol.

Table 1 also shows the kinetic parameters for the 0.5 M NaClO$_4$ (pH 10.66) PLL α-helix-like and π-helix (bulge) (un)folding. The α-helix-like unfolding activation energy is 21.9 ± 3.1 kcal/mol, while the folding activation energy is 2.5 ± 3.1 kcal/mol. The π-helix (bulge) unfolding activation energy is 23.2 ± 6.1 kcal/mol, while the folding activation energy is −0.5 ± 6.1 kcal/mol.

Kinetic UVRR of PLL in Pure Water. Figure 6 shows T-jump difference UVRR spectra of PLL in pure water at pH 10.66 at different delay times between the pump and probe
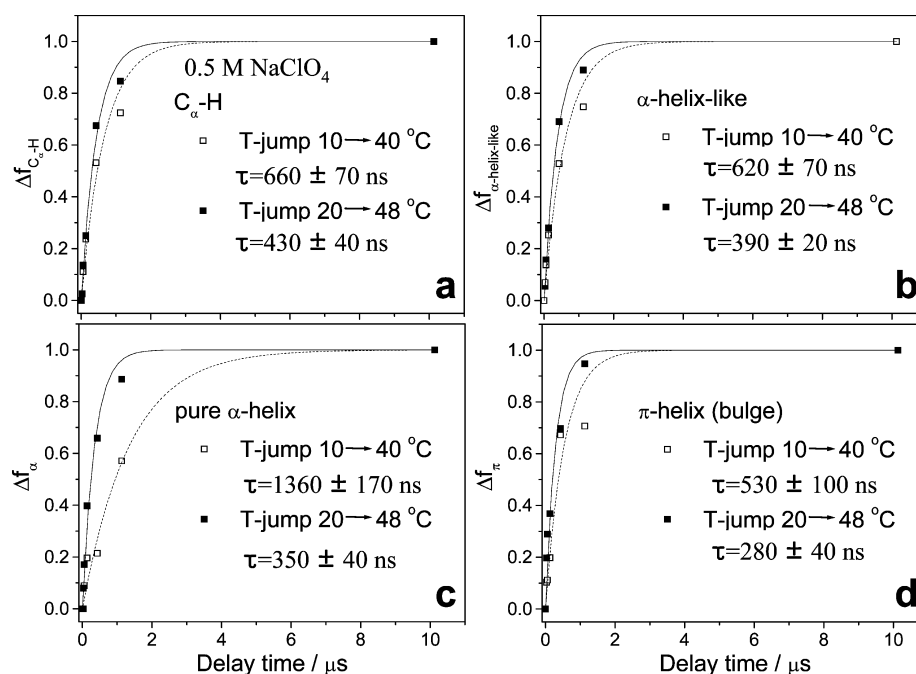
Figure 5. T-jump relaxation of the 0.5 M NaClO$_4$ (pH 10.66) (a) integrated C$_\alpha$−H band intensities, (b) the α-helix-like concentrations, (c) the pure α-helix concentrations, and (d) the π-helix (bulge) concentrations of PLL. Plotted are the C$_\alpha$−H band intensity change, $\Delta f_{C\alpha-H}$, the α-helix-like concentration change, $\Delta f_{\alpha\text{-helix-like}}$, the pure α-helix concentration change, Δf_α, and the π-helix (bulge) concentration change, Δf_π, from time zero to delay time t, relative to the change from static initial temperature to static final T-jump temperature. The dashed and solid curves are monoexponential fits for the 10 to 40 °C T-jump and the 20 to 48 °C T-jump, respectively.

Table 1. Kinetic Parameters for the 0.5 M NaClO$_4$ (pH 10.66) PLL α-Helix-like Conformations, the Pure α-Helix, and the π-Helix (Bulge) (Un)folding

		final T-jump temp		activation energy, $G^\ddagger$/kcal/mol
		40 °C	48 °C	
α-helix-like	equilibrium constant, $K_{helical} = f_{extend}{}^a/f_{helical}$	0.68 ± 0.03	1.45 ± 0.06	
	$\Delta G_{helical}{}^b = -RT(\ln K_{helical})$/kcal/mol	0.24 ± 0.03	−0.23 ± 0.03	
	relaxation rate, τ/ns	620 ± 70	390 ± 20	
	folding time, $\tau_f = (k_f)^{-1}$/ns	1040 ± 110	940 ± 50	2.5 ± 3.1
	unfolding time, $\tau_u = (k_u)^{-1}$/ns	1540 ± 170	650 ± 40	21.9 ± 3.1
pure α-helix	equilibrium constant, $K_\alpha = f_{extend}/f_\alpha$	2.03 ± 0.08	5.01 ± 0.21	
	$\Delta G_\alpha{}^b = -RT(\ln K_\alpha)$/kcal/mol	−0.44 ± 0.03	−1.03 ± 0.03	
	relaxation rate/ns	1350 ± 170	350 ± 40	
	folding time/ns	4100 ± 510	2090 ± 230	17.2 ± 4.2
	unfolding time/ns	2020 ± 250	420 ± 50	40.4 ± 4.2
π-helix (bulge)	equilibrium constant, $K_\pi = f_{extend}/f_\pi$	1.47 ± 0.06	3.69 ± 0.15	
	$\Delta G_\pi{}^b = -RT(\ln K_\pi)$/kcal/mol	−0.24 ± 0.03	−0.83 ± 0.03	
	relaxation rate/ns	530 ± 100	280 ± 40	
	folding time/ns	1310 ± 240	1330 ± 210	−0.5 ± 6.1
	unfolding time/ns	890 ± 160	360 ± 60	23.2 ± 6.1

$^a f_{extend}$ refers to the concentration of the extended PPII and 2.5$_1$-helix conformations. $^b \Delta G_{helical}$ is the free energy difference between the PPII and 2.5$_1$-helix conformations and the α-helix-like conformations. ΔG_α is the free energy difference between the PPII and 2.5$_1$-helix conformations and the pure α-helix. ΔG_π is the free energy difference between the PPII and 2.5$_1$-helix conformations and the π-helix (bulge).

laser pulses. The static 10 and 20 °C spectra in pure water show significantly increased C$_\alpha$−H band intensities relative to those in 0.5 M NaClO$_4$ (Figure 2), indicating significantly decreased PLL α-helical content in pure water compared to that in 0.5 M NaClO$_4$.[33] The 28 ns difference spectra show small positive features in the AmIII$_3$ region and slightly negative features in the C$_\alpha$−H region (that result from the temperature dependence of the hydrogen bonding between water and the peptide bond amide nitrogens.[37]) As the delay time increases, the positive features in the AmIII$_3$ and C$_\alpha$−H region increase,

indicating α-helix melting.[34] The spectral evolution for the 20 to 54 °C T-jump is complete within 1128 ns, faster than the 10 to 44 °C T-jump.

Transient Ψ Distributions. Figure 7 shows the delay time dependent Ramachandran Ψ probability distributions for PLL in pure water (pH 10.66). The static 10 °C Ψ distribution shows contributions of the π-helix (bulge) ($\Psi \sim -70$ °), the pure α-helix ($\Psi \sim -40$ °), type I/I′ or type II/II′ β turns (T1, $\Psi \sim 5$ °), and type III′ β turn or inverse γ turn (T2, $\Psi \sim 50$ °). It also contains contributions of the PPII-like ($\Psi \sim 140$ °) and
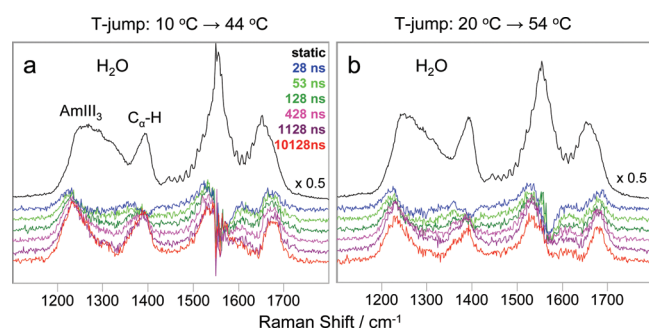
Figure 6. T-jump difference UVRR spectra of PLL in pure water (pH 10.66) at different delay times between the pump and probe laser pulses. These difference spectra were obtained by subtracting the static initial temperature spectrum from each of the longer delay time spectra. (a) Difference spectra for a T-jump from 10 to 44 °C. (b) Difference spectra for a T-jump from 20 to 54 °C. All spectra were normalized to the ~3400 cm^{-1} water stretching band intensities before spectral subtraction. The oscillations centered around 1550 cm^{-1} result from the rotational bands of oxygen.[35,36] The 10 °C AmII mode region contains oxygen stretching band contribution at ~1550 cm^{-1} that is not fully subtracted out. This narrow feature gives rise to an apparent AmII narrowing.

2.5$_1$-helix ($\Psi \sim 170$ °) conformations. For the 10 to 44 °C T-jump, the π-helix (bulge) and pure α-helix concentrations slightly decrease at 28 ns and further decrease at longer delay
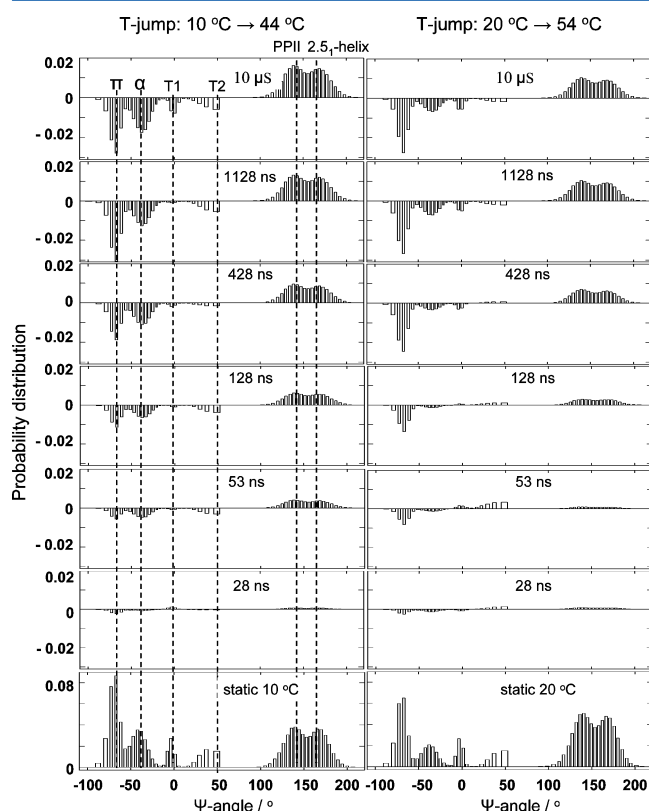

Figure 7. Ramachandran Ψ probability distributions for PLL at 10 and 20 °C in pure water (pH 10.66). Delay time dependent difference Ramachandran Ψ probability distributions for PLL in pure water (pH 10.66). These difference Ψ distributions were obtained by subtracting the static initial temperature Ψ distribution from each of the longer delay time Ψ distributions. π: π-helix (bulge). α: pure α-helix. T1 and T2: turns.

times. The T1 turn concentration slightly increases at 28 ns and then slightly decreases as the delay time increases (Figure 8).
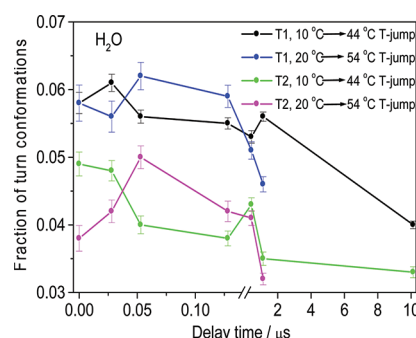

Figure 8. Delay time dependent fractions of T1 and T2 turn conformations of PLL in pure water at pH 10.66.

The T2 turn concentration starts decreasing at 28 ns, then increases at 428 ns, and decreases again at 1128 ns (Figure 8). The PPII and 2.5$_1$-helix concentrations monotonically increase as the delay time increases.

The static 20 °C Ψ distribution shows decreased α-helix-like concentrations and increased PPII and 2.5$_1$-helix concentrations, relative to those at 10 °C (Figure 7). For the 20 to 54 °C T-jump, the π-helix (bulge) and pure α-helix concentrations decrease at 28 ns and further decrease at longer delay times. The T1 concentration slightly increases at 53 ns and starts decreasing again at 428 ns (Figure 8). The T2 concentration starts increasing at 28 ns and then starts decreasing at 128 ns (Figure 8). The PPII and 2.5$_1$-helix concentrations increase as the delay time increases.

Relaxation Rates. Figure 9 shows monoexponential fits, $\Delta f = 1 - \exp(-t/\tau)$ to the pure water (pH 10.66) relaxation of the integrated C$_\alpha$−H band intensities (Figure 9a), the α-helix-like ($\pi + \alpha +$ T1 + T2) concentrations (Figure 9b), the pure α-helix concentrations (Figure 9c), and the π-helix (bulge) concentrations of PLL (Figure 9d).

We find a C$_\alpha$−H relaxation time for the 10 to 44 °C T-jump of 430 ± 90 ns (which is similar to that measured by JiJi et al.;[39] however, they performed UVRR T-jump experiments of PLL at pH 11.6, and their results were complicated by PLL β-sheet formation), whereas for the 20 to 54 °C T-jump, the relaxation time is 330 ± 30 ns. We also find an α-helix-like relaxation time for the 10 to 44 °C T-jump of 410 ± 80 ns, whereas for the 20 to 54 °C T-jump, the relaxation time is 370 ± 20 ns. The pure α-helix relaxation time for the 10 to 44 °C T-jump is 390 ± 90 ns, whereas for the 20 to 54 °C T-jump, the relaxation time is 500 ± 90 ns. The π-helix (bulge) relaxation time for the 10 to 44 °C T-jump is 310 ± 40 ns, whereas for the 20 to 54 °C T-jump, the relaxation time is 180 ± 10 ns.

Kinetic Parameters. Table 2 shows that the reciprocals of the pure water PLL pure α-helix unfolding rate constants are essentially the same of 450 ± 104 ns (at 44 °C) and 550 ± 110 ns (at 54 °C), while the reciprocals of the folding rate constant slows from 2900 ± 680 ns (at 44 °C) to 5540 ± 1000 ns (at 54 °C).

Table 2 also shows the kinetic parameters for the pure water PLL α-helix-like, the pure α-helix, and the π-helix (bulge) (un)folding. The α-helix-like unfolding activation energy is 4.2 ± 4.0 kcal/mol, while the folding activation energy is −3.1 ± 4.0 kcal/mol. The pure α-helix unfolding activation energy is −4.2 ± 6.0 kcal/mol, while the folding activation energy is
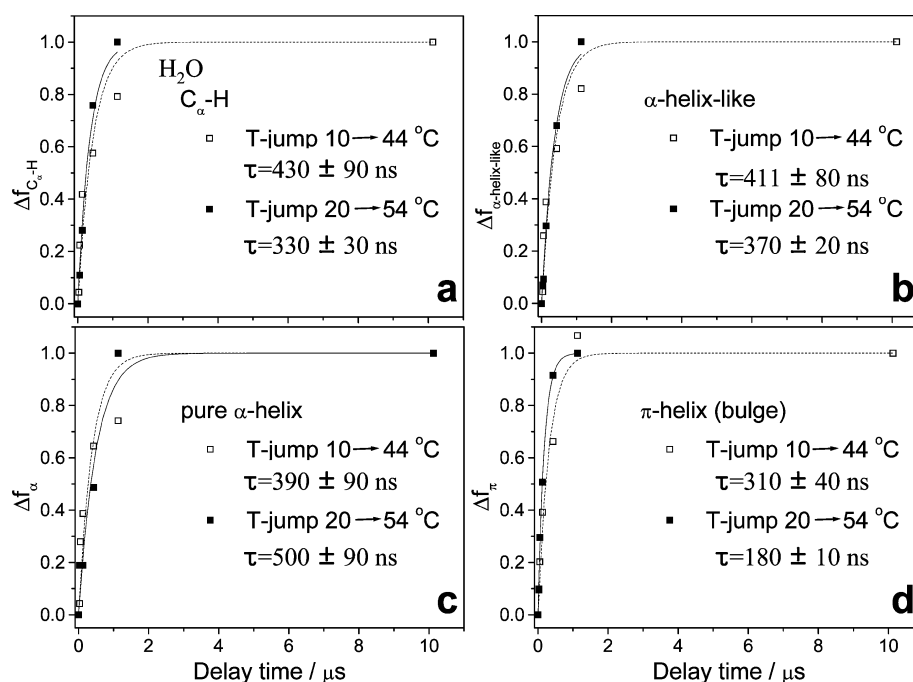
Figure 9. T-jump relaxation of the pure water (pH 10.66) (a) integrated $C_\alpha-H$ band intensities, (b) the α-helix-like concentrations, (c) the pure α-helix concentrations, and (d) the π-helix (bulge) concentrations of PLL. Plotted are the $C_\alpha-H$ band intensity change, $\Delta f_{C\alpha-H}$, the α-helix-like concentration change, $\Delta f_{\alpha\text{-helix-like}}$, the pure α-helix concentration change, Δf_α, and the π-helix (bulge) concentration change, Δf_π, from time zero to delay time t, relative to the change from static initial temperature to static final T-jump temperature. The dashed and solid curves are monoexponential fits for the 10 to 44 °C T-jump and the 20 to 54 °C T-jump, respectively. We calculated the $C_\alpha-H$ band intensities at time zero after T-jumps by using the measured static initial temperature $C_\alpha-H$ band intensities and the temperature dependence of the PPII and 2.5_1-helix $C_\alpha-H$ band intensities.[38] The conformational evolution for the 20 to 54 °C T-jump is complete within 1128 ns.

Table 2. Kinetic Parameters for the Pure Water (pH 10.66) PLL α-Helix-like Conformations, the Pure α-Helix, and the π-Helix (Bulge) (Un)folding

		final T-jump temp		
		44 °C	54 °C	activation energy, $G^\ddagger$/kcal/mol
α-helix-like	equilibrium constant, $K_{helical} = f_{extend}/f_{helical}$	1.98 ± 0.04	2.83 ± 0.07	
	$\Delta G_{helical} = -RT(\ln K_{helical})$/kcal/mol	−0.43 ± 0.02	−0.68 ± 0.02	
	relaxation rate, τ/ns	410 ± 80	370 ± 20	
	folding time, $\tau_f = (k_f)^{-1}$/ns	1210 ± 230	1410 ± 80	−3.1 ± 4.0
	unfolding time, $\tau_u = (k_u)^{-1}$/ns	610 ± 120	500 ± 30	4.2 ± 4.0
pure α-helix	equilibrium constant, $K_\alpha = f_{extend}/f_\alpha$	6.51 ± 0.15	10.1 ± 0.3	
	$\Delta G_\alpha = -RT(\ln K_\alpha)$/kcal/mol	−1.18 ± 0.02	−1.50 ± 0.02	
	relaxation rate/ns	390 ± 90	500 ± 90	
	folding time/ns	2900 ± 680	5540 ± 1000	−13.1 ± 6.0
	unfolding time/ns	450 ± 100	550 ± 100	−4.2 ± 6.0
π-helix (bulge)	equilibrium constant, $K_\pi = f_{extend}/f_\pi$	4.12 ± 0.09	6.54 ± 0.17	
	$\Delta G_\pi = -RT(\ln K_\pi)$/kcal/mol	−0.89 ± 0.02	−1.22 ± 0.02	
	relaxation rate/ns	310 ± 40	180 ± 10	
	folding time/ns	1580 ± 200	1340 ± 80	3.5 ± 2.7
	unfolding time/ns	380 ± 50	200 ± 10	12.8 ± 2.7

−13.1 ± 6.0 kcal/mol. This negative folding activation energy indicates a failure of two-state modeling of the PLL pure α-helix (un)folding kinetics. The π-helix (bulge) unfolding activation energy is 12.8 ± 2.7 kcal/mol, while the folding activation energy is 3.5 ± 2.7 kcal/mol.

■ DISCUSSION

We utilize T-jump UVRR to monitor PLL unfolding kinetics of the α-helix-like conformations (including the pure α-helix, π-helix (bulge), and turns), the pure α-helix, and the π-helix (bulge). The relaxation rate of the α-helix-like conformations of

PLL in pure water is slower than that of the α-helix-like conformations of alanine-based peptides due to the slower PLL unfolding that dominates the relaxation kinetics.[17,18]

The PLL pure α-helix folding time is similar to that of alanine-based peptides.[17,18] PLL has ≥69 residues, much longer than ~20 residue alanine-based peptides. This result is consistent with the idea that α-helix nucleation is the rate limiting step during α-helix folding, while α-helix propagation is fast.

Turn Conformations Are Intermediates in PLL Unfolding. Previous studies proposed that turn conformations

Table 3. Pure α-Helix and π-Helix (Bulge) Unfolding and Folding Times for an Alanine Peptide and PLL at Different Final T-jump Temperatures

		unfolding time/ns		folding time/ns	
	final T-jump temp	pure α-helix	π-helix (bulge)	pure α-helix	π-helix (bulge)
$A_5(A_3RA)_3A$ in pure water	40 °C	677 ± 230^a	61 ± 18^a	3553 ± 1207^a	$\geq 61^a$
PLL in pure water (pH 10.66)	44 °C	450 ± 100	380 ± 50	2900 ± 680	1580 ± 200
PLL in 0.5 M NaClO$_4$ (pH 10.66)	40 °C	2020 ± 250	890 ± 160	4100 ± 510	1310 ± 240
	48 °C	420 ± 50	360 ± 60	2090 ± 230	1330 ± 210

^{a}Results of Mikhonin et al.[18]

are intermediates during α-helix melting.[40−42] We observe that, for the 20 to 48 °C T-jump in 0.5 M NaClO$_4$, the type I/I′ or type II/II′ β turn ($\Psi \sim 5°$) concentrations increase at 28 ns, as the α-helix and π-helix (bulge) concentrations decrease (Figure 3). However, the PPII and 2.5$_1$-helix concentrations increase little at 28 ns. This indicates that type I/I′ or type II/II′ β turns may be α-helix and π-helix (bulge) unfolding intermediates in the presence of ClO$_4^-$. Their concentrations accumulate at short delay times.

In contrast, for the 20 to 54 °C T-jump in pure water, the type III′ β turn or inverse γ turn ($\Psi \sim 50°$) may be intermediates because their concentrations increase at 28 and 53 ns (Figure 7), as the α-helix and π-helix (bulge) concentrations decrease. Again, the PPII and 2.5$_1$-helix concentrations increase little at these short delay times. These results suggest that the unfolding intermediates differ between pure water and in ClO$_4^-$ solution.

π Helix (Bulge) Unfolds and Refolds Faster than the α Helix. Previous studies of an alanine-based peptide indicated that the π bulge unfolding and folding times at 40 °C are ~12-fold faster than those of the pure α-helix (Table 3).

We observe for PLL that the π-helix (bulge) unfolding time at 40 °C in 0.5 M NaClO$_4$ (pH 10.66) is twice as fast as that of the pure α-helix (Table 3). This may result from the fact the π-helix (bulge) hydrogen-bonding geometry is less optimized and weaker than that of the α-helix.[43,44]

In contrast, the π-helix (bulge) and pure α-helix unfolding times at 48 °C in 0.5 M NaClO$_4$ (pH 10.66) are similar. The PLL 44 °C pure water (pH 10.66) π-helix (bulge) unfolding time is similar to that of the pure α-helix.

The PLL π-helix (bulge) folding times are always faster than those of the pure α-helix (Table 3).

ClO$_4^-$ Lys Side Chain −NH$_3^+$—Peptide Backbone Binding Slows α-Helix (Un)folding. ClO$_4^-$ forms ion pairs between the Lys side chain −NH$_3^+$ groups and the peptide backbone[45−47] that decreases the electrostatic repulsion between side chain charges, thus stabilizing the α-helix. Previous molecular dynamics studies indicate that the α-helix (un)folding kinetics of an alanine-based peptide of sequence Ac−A(EAAAK)$_2$A−Nme is slowed by the ion binding to peptide charged groups.[23]

We calculated the PLL pure α-helix unfolding and folding times in 0.5 M NaClO$_4$ at 44 °C, by using eq 1 and the Table 1 kinetic parameters. The calculated pure α-helix unfolding time in 0.5 M NaClO$_4$ (pH 10.66) at 44 °C (Table 4) is twice as slow as that in pure water, while the folding times are the same. Thus, ClO$_4^-$ binding to Lys side chain −NH$_3^+$ groups and the peptide backbone slows α-helix unfolding, while not impacting α-helix folding, resulting in an increased α-helix stability.

ClO$_4^-$ Binding Increases (Un)folding Activation Barriers. Table 5 compares the PLL (un)folding activation barriers between 0.5 M NaClO$_4$ (pH 10.66) and pure water

Table 4. PLL Pure α-Helix Folding and Unfolding Times

	pure α-helix folding time/ns	pure α-helix unfolding time/ns
PLL in 0.5 M NaClO$_4$ (pH 10.66) at 44 °C	2890 ± 600^a	890 ± 180^a
PLL in pure water (pH 10.66) at 44 °C	2900 ± 680	450 ± 100

^{a}Calculated by using eq1 and Table 1 kinetic parameters.

Table 5. PLL (Un)folding Activation Energies

		PLL in pure water (pH 10.66)	PLL in 0.5 M NaClO$_4$ (pH 10.66)
unfolding activation energy/kcal/mol	α-helix-like	4.2 ± 4.0	21.9 ± 3.1
	pure α-helix	-4.2 ± 6.0	40.4 ± 4.2
	π-helix(bulge)	12.8 ± 2.7	23.2 ± 6.1
folding activation energy/kcal/mol	α-helix-like	-3.1 ± 4.0	2.5 ± 3.1
	pure α-helix	-13.1 ± 6.0^a	17.2 ± 4.2
	π-helix(bulge)	3.5 ± 2.7	-0.5 ± 6.1

^{a}The negative folding activation energy indicates a failure of two-state modeling.

(pH 10.66). In general, the unfolding activation barriers of PLL are much greater in the presence of ClO$_4^-$ than in pure water. In contrast, the α-helix-like and the π-helix (bulge) folding activation barriers in 0.5 M NaClO$_4$ are identical within experimental error to those in pure water. Interestingly, the pure water pure α-helix folding activation barrier is negative, possibly indicating the opening of additional folding pathway(s) as the temperature increases.

In ClO$_4^-$, the pure α-helix unfolding activation barrier is a maximum and positive. These results may indicate that ClO$_4^-$ preferentially binds to the PLL folded conformation, decreasing the energy of the folded conformation relative to the energy of the unfolded PPII and 2.5$_1$-helix conformations.

Ma et al. observed that NaClO$_4$ slows the H/D exchange rate of the PLL unfolded conformations and proposed that ClO$_4^-$ binding to the backbone and the Lys −NH$_3^+$ groups protects the backbone amide NH from exchange.[45] The ion pairing between ClO$_4^-$ and PLL is expected to be more stable in folded conformations than in unfolded conformations, partly because of the lower dielectric constant of the folded conformations in the region between the backbone and side chains. This region of unfolded PPII-like conformations is populated by the high dielectric constant water that hydrogen bonds to the backbone and Lys side chains.[48,49]

Do the PLL Folding and Unfolding Coordinates Differ? Figure 10 shows the reaction coordinate for PLL pure α-helix (un)folding in 0.5 M NaClO$_4$ (pH 10.66). The calculated pure α-helix unfolding activation energy, $G^{\ddagger}_{\alpha u}$, and
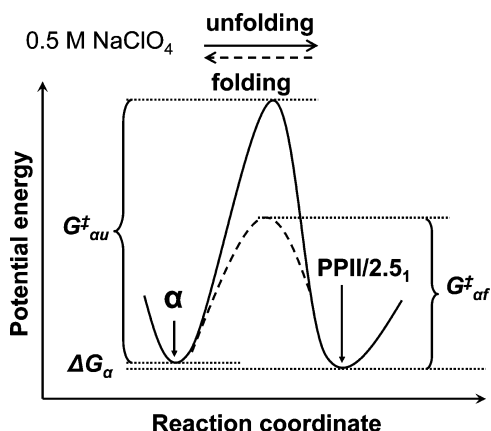
Figure 10. Two-state reaction coordinate for the 0.5 M NaClO$_4$ PLL pure α-helix (un)folding at 40 and 48 °C (pH 10.66). $G^{\ddagger}_{\alpha u}$ and $G^{\ddagger}_{\alpha f}$ are the pure α-helix unfolding and folding activation energies, respectively. ΔG_{α} is the free energy difference between the unfolded PPII/2.5$_1$-helix conformations and the pure α-helix.

folding activation energy, $G^{\ddagger}_{\alpha f}$, are 40.4 ± 4.2 kcal/mol and 17.2 ± 4.2 kcal/mol, respectively (Table 5).

The free energy differences between the unfolded conformations and the pure α-helix are small, with ΔG_{α} of −0.44 ± 0.03 kcal/mol and −1.03 ± 0.03 kcal/mol at 40 and 48 °C, respectively (Table 1). For a true two-state system, the α-helix unfolding energetics require $G^{\ddagger}_{\alpha u} = G^{\ddagger}_{\alpha f} + \Delta G_{\alpha}$ if the same reaction coordinate were followed. Thus, the system cannot be two-state and the α-helix folding coordinate must differ from the unfolding coordinate. This is not surprising, since it would be unlikely, for example, for the PPII and 2.5$_1$-helix to follow the identical folding pathways.

Figure 11 shows the reaction coordinate for PLL π-helix (bulge) (un)folding in 0.5 M NaClO$_4$ at pH 10.66. The
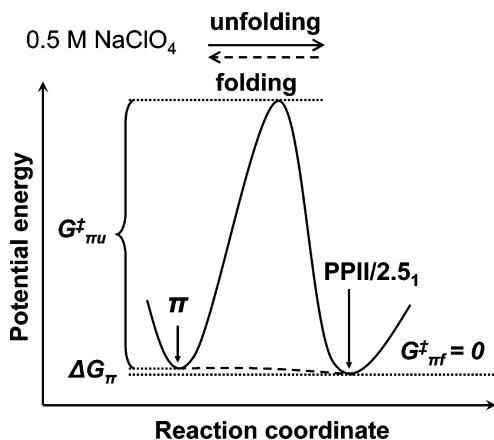

Figure 11. Two-state reaction coordinate for the 0.5 M NaClO$_4$ PLL π-helix (bulge) (un)folding at 40 and 48 °C (pH 10.66). $G^{\ddagger}_{\pi u}$ and $G^{\ddagger}_{\pi f}$ are the π-helix (bulge) unfolding and folding activation energies, respectively. ΔG_{π} is the free energy difference between the unfolded PPII/2.5$_1$-helix conformations and the π-helix (bulge).

calculated $G^{\ddagger}_{\pi u}$ and $G^{\ddagger}_{\pi f}$ are 23.2 ± 6.1 kcal/mol and −0.5 ± 6.1 kcal/mol, respectively (Table 5), with ΔG_{π} of −0.24 ± 0.03 kcal/mol and −0.83 ± 0.03 kcal/mol at 40 and 48 °C, respectively (Table 1). $G^{\ddagger}_{\pi u} \neq G^{\ddagger}_{\pi f} + \Delta G_{\pi}$; thus, the π-helix (bulge) folding and unfolding coordinates also differ.

A two-state modeling of the pure water PLL pure α-helix (un)folding kinetics (pH 10.66) shows a negative folding activation energy of −13.1 ± 6.0 kcal/mol (Table 5), clearly indicating that the PLL pure α-helix (un)folding in pure water is not a two-state process.

Figure 12 shows the pure water (pH 10.66) reaction coordinate for the PLL π-helix (bulge) (un)folding. The
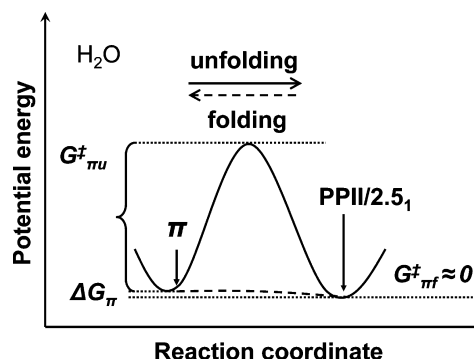

Figure 12. Two-state reaction coordinate for the pure water PLL π-helix (bulge) (un)folding at 44 and 54 °C (pH 10.66). $G^{\ddagger}_{\alpha u}$ and $G^{\ddagger}_{\alpha f}$ are the π-helix (bulge) unfolding and folding activation energies, respectively. ΔG_{α} is the free energy difference between the unfolded PPII/2.5$_1$-helix conformations and the π-helix (bulge).

calculated $G^{\ddagger}_{\pi u}$ and $G^{\ddagger}_{\pi f}$ are 12.8 ± 2.7 kcal/mol and 3.5 ± 2.7 kcal/mol, respectively (Table 5). ΔG_{π} are −0.89 ± 0.02 kcal/mol and −1.22 ± 0.02 kcal/mol at 44 and 54 °C, respectively (Table 2). $G^{\ddagger}_{\pi u} \neq G^{\ddagger}_{\pi f} + \Delta G_{\pi}$; thus, in pure water the π-helix (bulge) folding and unfolding coordinates differ.

Contribution of Ramachandran Ψ Angle to α-Helix and π-Helix (Bulge) (Un)folding Reaction Coordinate. By using the methodology of Ma et al.,[24] we calculated the Ramachandran Ψ angle probability distributions, and by assuming Boltzmann distributions, we then calculated the projection of the Gibbs free energy landscapes for PLL in 0.5 M NaClO$_4$ along the Ramachandran Ψ angle coordinate (Figure 13). The 40 °C energy landscape (Figure 13) shows an α-helix-like basin where the π-helix (bulge) free energy is lowest and the pure α-helix and turn conformations occur at higher energies. The Gibbs free energy landscape also contains an unfolded basin consisting of PPII and 2.5$_1$-helix conformations. As the temperature increases to 48 °C, the α-helix-like basin
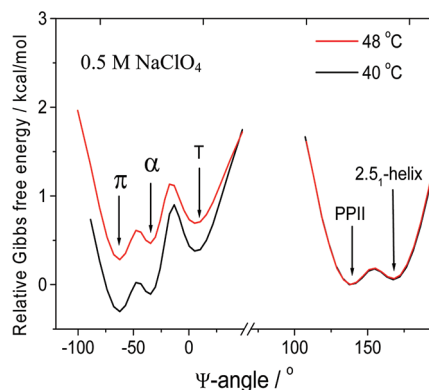

Figure 13. Calculated projection of the Gibbs free energy landscapes for PLL in 0.5 M NaClO$_4$ at pH 10.66, along the Ramachandran Ψ angle coordinate. PPII is the reference state.

free energies increase relative to that of the PPII and 2.5$_1$-helix unfolded basin.

The π-helix (bulge) free energy minimum is determined to be 0.19 ± 0.01 kcal/mol below that of the pure α-helix. The energy barriers along the Ψ angle coordinate between the π-helix (bulge) minimum and the pure α-helix conformation and between the pure α-helix minimum and the π-helix (bulge) conformation are 0.33 ± 0.02 kcal/mol and 0.14 ± 0.01 kcal/mol, respectively (Figure 13). This predicts that the unfolding activation barrier between the π-helix (bulge) and the PPII/2.5$_1$-helix conformation is ~0.3 kcal/mol more than that between the pure α-helix and the PPII/2.5$_1$-helix, while the folding activation barrier between the PPII/2.5$_1$-helix and the π-helix (bulge) folding is ~0.1 kcal/mol more than that between the PPII/2.5$_1$-helix and the pure α-helix, if the α-helix and π-helix (bulge) (un)folding were constrained to evolve along the Ψ angle coordinate. However, the PLL π-helix (bulge) unfolding and folding activation energies in 0.5 M NaClO$_4$ (Table 5) are both calculated to be many kilocalories per mole less than those of pure α-helices. This indicates that the π-helix (bulge) unfolding and folding are not constrained to pass through the α-helix well and must instead involve a reaction coordinate(s) other than a pure Ψ angle reaction coordinate.

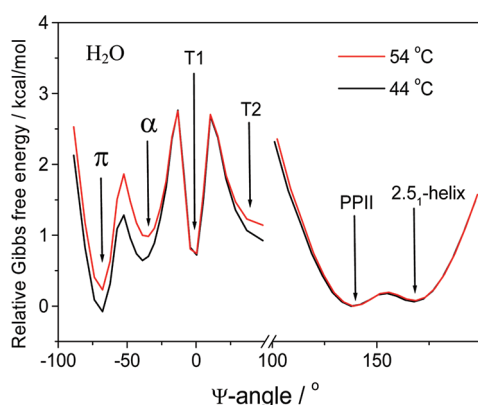We also calculated the Gibbs free energy landscapes for PLL in pure water at pH 10.66 (Figure 14). The 44 °C energy

Figure 14. Calculated projection of the Gibbs free energy landscapes for PLL in pure water at pH 10.66, along the Ramachandran Ψ angle coordinate. PPII is the reference state.

landscape shows an α-helix-like basin where the π-helix (bulge) free energy is lowest, followed by the pure α-helix and T1 and T2 turn conformations. As the temperature increases to 54 °C, the α-helix-like basin free energies increase relative to that of the PPII/2.5$_1$-helix basin.

A similar situation occurs for PLL in pure water. In pure water, the π-helix (bulge) free energy is 0.74 ± 0.02 kcal/mol below that of the pure α-helix. The energy barriers along the Ψ angle coordinate between the π-helix (bulge) minimum and the pure α-helix conformation and between the pure α-helix minimum and the π-helix (bulge) conformation are 1.5 ± 0.2 kcal/mol and 0.76 ± 0.17 kcal/mol, respectively (Figure 14). This predicts that the unfolding activation barrier between the π-helix (bulge) and the PPII/2.5$_1$-helix is ~1.5 kcal/mol more than that between the pure α-helix and the PPII/2.5$_1$-helix, while the folding activation barrier between the PPII/2.5$_1$-helix and the π-helix (bulge) is ~0.76 kcal/mol more than that between the PPII/2.5$_1$-helix and the pure α-helix, if the α-helix and π-helix (bulge) (un)folding were constrained to evolve

along the Ψ angle coordinate. However, two-state modeling indicates that the PLL π-helix (bulge) unfolding and folding activation energies in pure water are significantly greater than those of the pure α-helix (Table 5). This indicates that the π-helix (bulge) unfolding and folding does not go through the α-helix energy well.

These results clearly demonstrate that PLL (un)folding differs dramatically from a two-state process.

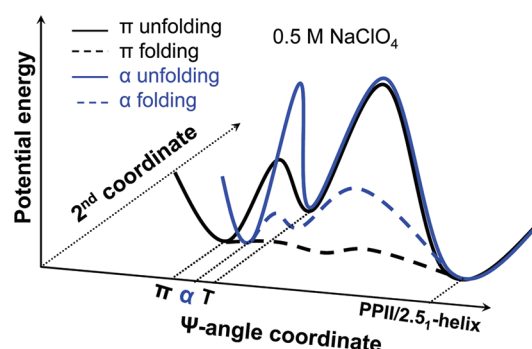**PLL (Un)folding Reaction Coordinate.** Figure 15 shows a multistate reaction coordinate for the 0.5 M NaClO$_4$ PLL π-

Figure 15. Multistate reaction coordinate for the 0.5 M NaClO$_4$ (pH 10.66) PLL π-helix (bulge) and pure α-helix unfolding and folding at 40 and 48 °C.

helix (bulge) and pure α-helix (un)folding. Type I/I′ or type II/II′ β turns are indicated to be π-helix (bulge) and α-helix unfolding intermediates. The π-helix (bulge) unfolding and folding do not dominantly go through the α-helix energy well but involves at least one additional reaction coordinate. The π-helix (bulge) and pure α-helix folding coordinates differ from their unfolding coordinates.

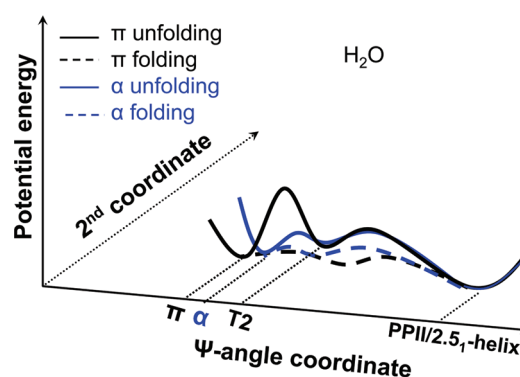Figure 16 shows a multistate reaction coordinate for the pure water (pH 10.66) PLL π-helix (bulge) and pure α-helix

Figure 16. Multistate reaction coordinate for pure water (pH 10.66) PLL π-helix (bulge) and pure α-helix unfolding and folding at 44 and 54 °C.

(un)folding. Type III′ β turn or inverse γ turn (T2) are shown as π-helix (bulge) and α-helix unfolding intermediates. The π-helix (bulge) unfolding and folding do not directly go through the α-helix energy well but involve a second reaction coordinate. The π-helix (bulge) and pure α-helix folding coordinates also differ from their unfolding coordinates.

Implication for Salt Effects on Peptide (Protein) Stability in General. Previous studies have demonstrated

that ions can impact peptide (protein) stability by preferentially binding to peptide (protein) side chains to form ion pairs.[50,51] Ions can also screen electrostatic interactions between peptide (protein) charges.[34] Another potential mechanism that could impact peptide (protein) conformation could occur by the impact of ions on the water solvent properties that control peptide (protein) hydration.[52,53]

The model of Collins et al.'s matching water affinities predicts that preferential ion pair formation occurs between oppositely charged ions of similar charge densities.[50,51,54] Thus, for PLL, we expect that low charge density ClO_4^- preferentially binds to Lys side chain $-NH_3^+$ groups and the peptide backbone. We observe that ClO_4^- binding slows the PLL α-helix unfolding rate compared to that in pure water but little impacts the folding rate, resulting in an increased α-helix stability. ClO_4^- binding also significantly increases the PLL unfolding activation barrier but little impacts the folding barrier. Ramajo et al. studied the electrostatic screening effect of NaCl on the folding dynamics of a mainly polyala peptide.[22] They observed a decreased α-helix relaxation time in 0.5 M NaCl relative to that in pure water, which they ascribed to an increased α-helix folding rate. Little is known about the impact of ions on protein (peptide) (un)folding kinetics. More work is needed for us to better understand salt effects on peptide (protein) stability.

CONCLUSION

We utilize T-jump UVRR to monitor the (un)folding kinetics of the pure α-helix and the π-helix (bulge). We observe that the relaxation rates of folded conformations (including the π-helix (bulge), pure α-helix, and turns) of PLL are slower than those of alanine-based peptides. We also for the first time experimentally observe that turn conformations are α-helix and π-helix (bulge) unfolding intermediates. Turn conformations must have slower kinetics than the α-helix and π-helix (bulge) kinetics, resulting in relative turn concentration increases during high temperature α-helix and π-helix (bulge) unfolding.

The π-helix (bulge) melts before the α-helix in 0.5 M NaClO$_4$ (pH 10.66) at 40 °C. ClO_4^- binding to the Lys side chain $-NH_3^+$ groups and backbone peptide bonds slows pure α-helix unfolding but little impacts folding, resulting in an increased α-helix stability. ClO_4^- binding increases the PLL unfolding activation barrier but little impacts the folding barrier. The PLL folding reaction coordinate differs from the unfolding coordinate. The π-helix (bulge) unfolding and folding do not directly go through the α-helix basin. Our results clearly demonstrate that PLL (un)folding is far from a two-state process.

ASSOCIATED CONTENT

S Supporting Information

204 nm excited water stretching bands and difference spectra, T-jump calibration curve, 204 nm excited water stretching bands of 5 mg/mL PLL in 0.5 M NaClO$_4$ and with 0.015 M NaBr with and without IR pulses at 10 and 20 °C, 204 nm excited water stretching bands of 15 mg/mL PLL in water with and without IR pulses at 20 °C, molar absorptivity of NaBr in water, temperature dependence of 204 nm excited UVRR spectra of 1 mg/mL PLL in water at pH 10.65, and further references. This material is available free of charge via the Internet at http://pubs.acs.org.

AUTHOR INFORMATION

Corresponding Author

*E-mail: asher@pitt.edu.

Present Address

‡Department of Chemistry, Northwestern University, Evanston, Illinois 60208, United States

Notes

The authors declare no competing financial interest.

REFERENCES

(1) Baldwin, R. L.; Rose, G. D. *Trends Biochem. Sci.* **1999**, *24*, 26−33.

(2) Baldwin, R. L.; Rose, G. D. *Trends Biochem. Sci.* **1999**, *24*, 77−83.

(3) Dobson, C. M. *Philos. Trans. R. Soc., B* **2001**, *356*, 133−145.

(4) Dobson, C. M.; Sali, A.; Karplus, M. *Angew. Chem. Int. Ed.* **1998**, *37*, 868−893.

(5) Jahn, T. R.; Radford, S. E. *FEBS J.* **2005**, *272*, 5962−5970.

(6) Lindberg, M. O.; Oliveberg, M. *Curr. Opin. Struct. Biol.* **2007**, *17*, 21−29.

(7) Daggett, V.; Fersht, A. *Nat. Rev. Mol. Cell Biol.* **2003**, *4*, 497−502.

(8) Ihalainen, J. A.; Bredenbeck, J.; Pfister, R.; Helbing, J.; Chi, L.; van Stokkum, I. H. M.; Woolley, G. A.; Hamm, P. *Proc. Natl. Acad. Sci. U.S.A.* **2007**, *104*, 5383−5388.

(9) Bredenbeck, J.; Helbing, J.; Kumita, J. R.; Woolley, G. A.; Hamm, P. *Proc. Natl. Acad. Sci. U.S.A.* **2005**, *102*, 2379−2384.

(10) Huang, C. Y.; Getahun, Z.; Zhu, Y. J.; Klemke, J. W.; DeGrado, W. F.; Gai, F. *Proc. Natl. Acad. Sci. U.S.A.* **2002**, *99*, 2788−2793.

(11) Dyer, R. B.; Gai, F.; Woodruff, W. H. *Acc. Chem. Res.* **1998**, *31*, 709−716.

(12) Balakrishnan, G.; Hu, Y.; Bender, G. M.; Getahun, Z.; DeGrado, W. F.; Spiro, T. G. *J. Am. Chem. Soc.* **2007**, *129*, 12801−12808.

(13) Williams, S.; Causgrove, T. P.; Gilmanshin, R.; Fang, K. S.; Callender, R. H.; Woodruff, W. H.; Dyer, R. B. *Biochemistry* **1996**, *35*, 691691−697.

(14) Thompson, P. A.; Eaton, W. A.; Hofrichter, J. *Biochemistry* **1997**, *36*, 9200−9210.

(15) Thompson, P. A.; Munoz, V.; Jas, G. S.; Henry, E. R.; Eaton, W. A.; Hofrichter, J. *J. Phys. Chem. B* **2000**, *104*, 378−389.

(16) Huang, C. Y.; Klemke, J. W.; Getahun, Z.; DeGrado, W. F.; Gai, F. *J. Am. Chem. Soc.* **2001**, *123*, 9235−9238.

(17) Lednev, I. K.; Karnoup, A. S.; Sparrow, M. C.; Asher, S. A. *J. Am. Chem. Soc.* **1999**, *121*, 8074−8086.

(18) Mikhonin, A.; Asher, S.; Bykov, S.; Murza, A. *J. Phys. Chem. B* **2007**, *111*, 3280−3292.

(19) Young, W. S.; Brooks, C. L. *J. Mol. Biol.* **1996**, *259*, 560−572.

(20) Chowdhury, S.; Zhang, W.; Wu, C.; Xiong, G. M.; Duan, Y. *Biopolymers* **2003**, *68*, 63−75.

(21) Wang, T.; Zhu, Y. J.; Getahun, Z.; Du, D. G.; Huang, C. Y.; DeGrado, W. F.; Gai, F. *J. Phys. Chem. B* **2004**, *108*, 15301−15310.

(22) Ramajo, A. P.; Petty, S. A.; Volk, M. *Chem. Phys.* **2006**, *323*, 11−20.

(23) von Hansen, Y.; Kalcher, I.; Dzubiella, J. *J. Phys. Chem. B* **2010**, *114*, 13815−13822.

(24) Ma, L.; Ahmed, Z.; Mikhonin, A. V.; Asher, S. A. *J. Phys. Chem. B* **2007**, *111*, 7675−7680.

(25) Tiffany, M. L.; Krimm, S. *Biopolymers* **1968**, *6*, 1379−1382.

(26) Painter, P. C.; Koenig, J. L. *Biopolymers* **1976**, *15*, 229−240.

(27) McColl, L. H.; Blanch, E. W.; Gill, A. C.; Rhie, A. G. O.; Ritchie, M. A.; Hecht, L.; Nielsen, K.; Barron, L. D. *J. Am. Chem. Soc.* **2003**, *125*, 10019−10026.

(28) Keiderling, T. A.; Silva, R. A. G. D.; Yoder, G.; Dukor, R. K. *Bioorg. Med. Chem.* **1999**, *7*, 133−141.

7111

dx.doi.org/10.1021/jp302007g | *J. Phys. Chem. B* 2012, 116, 7102−7112

(29) Bykov, S.; Lednev, I.; Ianoul, A.; Mikhonin, A.; Munro, C.; Asher, S. A. *Appl. Spectrosc.* **2005**, *59*, 1541−1552.

(30) Kubelka, J. *Photochem. Photobiol. Sci.* **2009**, *8*, 499−512.

(31) Mikhonin, A. V.; Ahmed, Z.; Ianoul, A.; Asher, S. A. *J. Phys. Chem. B* **2004**, *108*, 19020−19028.

(32) Myshakina, N. S.; Ahmed, Z.; Asher, S. A. *J. Phys. Chem. B* **2008**, *112*, 11873−11877.

(33) Wang, Y.; Purrello, R.; Jordan, T.; Spiro, T. G. *J. Am. Chem. Soc.* **1991**, *113*, 6359−6368.

(34) Xiong, K.; Asciutto, E. K.; Madura, J. D.; Asher, S. A. *Biochemistry* **2009**, *48*, 10818−10826.

(35) Fletcher, W. H.; Rayside, J. S. *J. Raman Spectrosc.* **1974**, *2*, 3−14.

(36) Weber, A.; McGinnis, E. A. *J. Mol. Spectrosc.* **1960**, *4*, 195−200.

(37) Asher, S.; Mikhonin, A.; Bykov, S. *J. Am. Chem. Soc.* **2004**, *126*, 8433−8440.

(38) Mikhonin, A. V.; Myshakina, N. S.; Bykov, S. V.; Asher, S. A. *J. Am. Chem. Soc.* **2005**, *127*, 7712−7720.

(39) JiJi, R. D.; Balakrishnan, G.; Hu, Y.; Spiro, T. G. *Biochemistry* **2006**, *45*, 34−41.

(40) Millhauser, G. L. *Biochemistry* **1995**, *34*, 10318−10318.

(41) Sundaralingam, M.; Sekharudu, Y. C. *Science* **1989**, *244*, 1333−1337.

(42) Millhauser, G. L.; Stenland, C. J.; Hanson, P.; Bolin, K. A.; vandeVen, F. J. M. *J. Mol. Biol.* **1997**, *267*, 963−974.

(43) Lee, K. H.; Benson, D. R.; Kuczera, K. *Biochemistry* **2000**, *39*, 13737−13747.

(44) Chapman, R.; Kulp, J. L.; Patgiri, A.; Kallenbach, N. R.; Bracken, C.; Arora, P. S. *Biochemistry* **2008**, *47*, 4189−4195.

(45) Ma, L.; Hong, Z.; Sharma, B.; Asher, S. *J. Phys. Chem. B* **2012**, *116*, 1134−1142.

(46) Ebert, G.; Kuroyanagi, Y. *Polymer* **1982**, *23*, 1147−1153.

(47) Ebert, G.; Kuroyanagi, Y. *Polymer* **1982**, *23*, 1154−1158.

(48) Shi, Z. S.; Olson, C. A.; Rose, G. D.; Baldwin, R. L.; Kallenbach, N. R. *Proc. Natl. Acad. Sci. U.S.A.* **2002**, *99*, 9190−9195.

(49) Shi, Z. S.; Chen, K.; Liu, Z. G.; Kallenbach, N. R. *Chem. Rev.* **2006**, *106*, 1877−1897.

(50) Collins, K. D. *Methods* **2004**, *34*, 300−311.

(51) Collins, K. D.; Neilson, G. W.; Enderby, J. E. *Biophys. Chem.* **2007**, *128*, 95−104.

(52) Collins, K. D.; Washabaugh, M. W. *Q. Rev. Biophys.* **1985**, *18*, 323−422.

(53) Zhang, Y. J.; Cremer, P. S. *Curr. Opin. Chem. Biol.* **2006**, *10*, 658−663.

(54) Collins, K. D. *Biophys. J.* **1997**, *72*, 65−76.